Atomic-Scale Structure and Stability of the $\sqrt{31} \times \sqrt{31}R9°$ Surface of $Al_2O_3(0001)$

J. V. Lauritsen,[1,*] M. C. R. Jensen,[1] K. Venkataramani,[1] B. Hinnemann,[2] S. Helveg,[2] B. S. Clausen,[2] and F. Besenbacher[1]

[1]*Interdisciplinary Nanoscience Center (iNANO) and Department of Physics and Astronomy, University of Aarhus, Denmark*

[2]*Haldor Topsøe A/S, Nymøllevej 55, 2800 Kongens Lyngby, Denmark*

(Received 23 April 2009; published 13 August 2009)

Through the interplay of noncontact atomic force microscopy studies and density functional theory calculations, an atomistic model for the $Al_2O_3(0001)$-$\sqrt{31} \times \sqrt{31}R9°$ surface reconstruction is revealed. The surface is found to consist of an Al adlayer on the Al_2O_3 substrate, and the driving force for the formation of the reconstruction is related to a detailed balance between strain in the adlayer and the preference for Al atoms to be located on distinct substrate sites.

DOI: 10.1103/PhysRevLett.103.076103 PACS numbers: 68.47.Gh, 68.35.B−, 68.35.Md, 68.37.Ps

The surface composition of ceramics is of utmost fundamental and technological importance as it controls the chemical and physical properties. Aluminum oxide (Al_2O_3), commonly referred to as alumina, is of special interest since it is considered as a replacement gate oxide in the microelectronics industry, as a substrate for the growth of functional thin films, and alumina is extensively used as support material for heterogeneous catalysts. However, despite numerous studies, the structural properties and chemistry on clean alumina surfaces are still matters of high controversy. Al_2O_3 exists in a number of polymorphs—transition aluminas—where the main difference is the detailed distribution of Al atoms coordinated to O in octahedral or tetrahedral sites [1]. However, even for the most stable phase—corundum (α-Al_2O_3)—the atomic-scale surface structure is not known in detail. Obtaining a complete picture is difficult since Al_2O_3 surfaces with a well-defined structure and stoichiometry are very difficult to prepare [2,3]. In addition, Al_2O_3 is an insulator with a band gap exceeding 8 eV, which severely restricts the use of surface sensitive methods. However, the atomic force microscope applied in the noncontact mode (nc-AFM) has recently evolved as a very powerful technique capable of providing atomic resolution imaging of insulating surfaces [4,5], including Al_2O_3 [6], in a quality comparable to that provided by the scanning tunneling microscope. Here we have used high-resolution nc-AFM to analyze the atomic-scale structure of the distinct $\sqrt{31} \times \sqrt{31}R9°$ reconstructed phase of the $Al_2O_3(0001)$ surface [2,3,7–9] formed by exposing a fresh corundum single crystal to high temperatures. In contrast to previous studies, we find that the $\sqrt{31} \times \sqrt{31}R9°$-$Al_2O_3(0001)$ surface consists of a single well-ordered overlayer of surface Al atoms placed on a bulk termination of Al_2O_3. Our density functional theory (DFT) calculations show that the driving force for formation of the reconstructed Al_2O_3 surface is due to a detailed balance between strain energies in the Al overlayer and the preference of Al to occupy distinct substrate sites.

The nc-AFM experiments were performed in an ultrahigh vacuum (UHV) chamber (pressure $<1 \times 10^{-10}$ mbar) using a beam deflection nc-AFM described elsewhere [10]. The measurements were performed by oscillating the AFM cantilever at its first resonance with constant amplitude and monitoring the frequency shift (df) as the tip was scanned across the surface. To provide the highest possible lateral resolution, the atom-resolved nc-AFM images were obtained in the constant height mode, i.e., by measuring the actual cantilever detuning (df) for a constant tip surface separation [6]. The reconstructed α-$Al_2O_3(0001)$ was prepared by heating a polished corundum single crystal (MTI Corporation) to 1500–1600 K under UHV. Surface cleanliness was investigated with x-ray photoelectron spectroscopy, and only peaks belonging to Al and O were detected. The DFT calculations were carried out with the DFT code DACAPO [11], which uses a plane-wave basis set and ultrasoft pseudopotentials [12]. As the exchange-correlation functional, the revised Perdew-Burke-Ernzerhoff functional was used [13]. An electronic temperature of 0.1 eV was used with Fermi smearing, and all energies were extrapolated to zero electronic temperature. For the calculations on the 1×1 unit cell, a plane-wave energy cutoff of 30 Ry and a density cutoff of 45 Ry have been used, and a slab with a thickness of six stoichiometric layers was used [14]. All atoms were relaxed until force components were below 0.03 eV/Å. The gas phase atmosphere is taken into account through the chemical potential formalism [15]. For the $\sqrt{31} \times \sqrt{31}R9°$ model, a lower energy cutoff of 25 Ry, density cutoff of 30 Ry, and Γ-point sampling were used. This model considers two stoichiometric layers, and all atoms were relaxed until all force components were below 0.16 eV/Å. Previous DFT studies on $Al_2O_3(0001)$ [14–18] have shown that, while the generalized gradient approximation (GGA) functional normally underestimates the band gap of insulators, the DFT-GGA scheme is able to predict surface properties in good agreement with experimental results.

Previous studies have reported that, when the $Al_2O_3(0001)$ surface is annealed under UHV conditions, the surface reconstructs compared to the simple $Al_2O_3(0001)$ (1×1) termination due to oxygen evaporation through intermediate structures [2,3,7,8] until a characteristic large hexagonal superstructure—the

$\sqrt{31} \times \sqrt{31}R9°$ reconstruction—forms at ~1500 K [8,17,19]. As depicted in Fig. 1(a), our nc-AFM images of the $\sqrt{31} \times \sqrt{31}R9°$-$Al_2O_3(0001)$ reconstructed surface reveal a rather complex, but atomically well-ordered surface structure. The long-range order of the surface is characterized by a 26.5 Å × 26.5 Å rhombic unit cell. Figure 1(b) shows a two-dimensional Fourier transform (FT) representation of the nc-AFM image, which is used to determine the atomic-scale distances and elucidate the rotation of the atomic lattice of the overlayer relative to the superstructure. The innermost white dot represents the $\sqrt{31} \times \sqrt{31}R9°$ superstructure (26.5 Å), whereas the outermost dark hexagon (yellow dots) reflects the hexagonal atomic structure with an average distance of 3.01 ± 0.07 Å. In addition to these main reflections, other, less intense FT reflections which are attributed to a noncommensurate structure within the unit cell also appear and satellite reflections due to the limited image size. From Fig. 1(b), it is determined that the atomic FT reflections are rotated by 23° clockwise with respect to the nearest reflection due to the superstructure, which, from previous studies [3], is known to be rotated further by 9° relative to the underlying substrate. Using this observation in a tentative epitaxial rotation model [19], a coincidence lattice with a correct $\sqrt{31} \times \sqrt{31}R9°$ structure is obtained by placing a "hypothetical" close-packed hexagonal atomic layer with a 3.01 Å lattice distance on top of the Al_2O_3 substrate and rotating by observed 23° + 9° = 32° [20]. The rotation reproduces the long-range order observed, but, as depicted in Fig. 2(a), the surface structure possesses a very pronounced internal pattern of substructures. As highlighted by black lines in Fig. 2(b), within each unit cell we can identify three distinct subdomains with short-range order which each appear with the 2.65 nm periodicity. As shown in detail in Fig. 3, domain **1** is characterized by a dark nc-AFM contrast, and its boundary consists of three triangles positioned in a slightly shifted manner. Domain **2**, which also appears with a dark nc-AFM contrast, consists of four interconnected hexagons that form a *Y* shape surrounded by a brighter rim. Domain **3** is imaged with a brighter nc-AFM contrast and with a boundary indicated by a larger triangle. Since nc-AFM is very sensitive to vertical displacements of atoms on the picometer scale, we can explain the contrast differences between the domains by small geometric variations in the atomic surface topography. The origin of the different geometric relaxations observed in three domains is then tentatively explained by the lattice mismatch and rotation of the Al overlayer, which inevitably places overlayer atoms in periodically modulated stacking domains with changing atom relaxations on different substrate sites. In principle, the atomic-scale nc-AFM contrast may for special tip terminations be further modulated by different affinities for the tip apex to interact with "chemically" different species on the surface [10]. However, in the present experiments we observed no significant differences in the AFM contrast among the three domains for different AFM tips, and large tip-dependent contrast differences deviating from the geometry of the surface are not expected to arise for surfaces that expose only one type of atom.

In α-Al_2O_3, the O atoms are arranged in a hexagonal close-packed lattice with Al atoms occupying two out of three octahedrally coordinated interstitial sites in between stacked oxygen planes. The (0001) surface terminates a *R*-Al-Al-O-Al-Al-O-*R* bulk stacking sequence [see Fig. 4(a)], and three simple terminations are possible: (i) the oxygen terminated O-*R*, (ii) the Al-O-*R* with Al in one of three possible octahedral sites [only Al_1 in

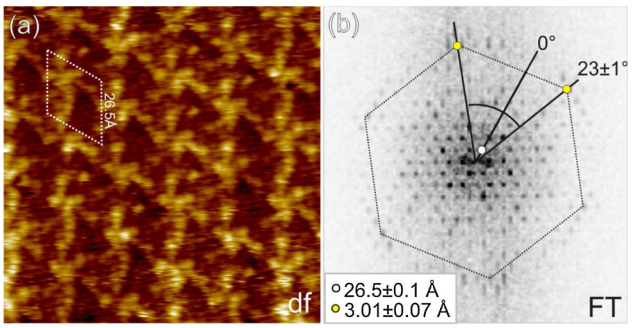

FIG. 1 (color online). (a) Constant height (df) nc-AFM image (90×90 Å^2) of the $\sqrt{31} \times \sqrt{31}R9°$-$Al_2O_3(0001)$ surface. Imaging parameters: $df_{set} = -20$ Hz, $A_{p-p} = 20$ nm, $f_0 = 330$ kHz, and $k = 44$ N/m. The dark/bright contrast reflects a df range of ±12 Hz. (b) 2D Fourier transform image. The angle indicates the rotation of the atomic lattice relative to the superstructure.

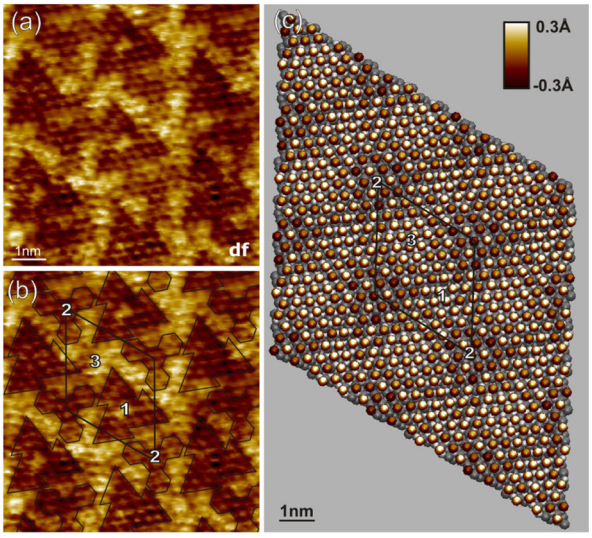

FIG. 2 (color online). (a) Constant height atom-resolved nc-AFM image (40×40 Å^2) of the $\sqrt{31} \times \sqrt{31}R9°$-$Al_2O_3(0001)$ surface. Image parameters: $df_{set} = -24$ Hz and df contrast: ±13 Hz. (b) The superimposed black lines outline the three types of subdomains. (c) Calculated model of the $\sqrt{31} \times \sqrt{31}R9°$ structure. Vertical relaxations are illustrated by a brown-white color scale. Substrate (Al-Al-O-*R*) atoms are shown as O (gray) and Al (light gray).

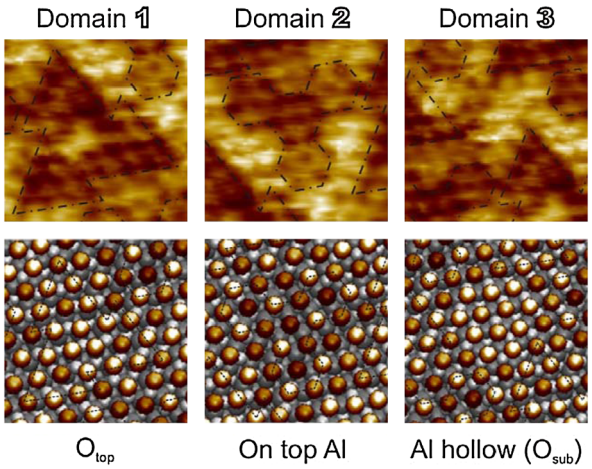

FIG. 3 (color online). Upper part: Zoom-in nc-AFM images of the three types of stacking domains contained in the $\sqrt{31} \times \sqrt{31}R9°$ structure. Lower part: Ball model of the corresponding stacking domains obtained from Fig. 2(c).

Fig. 4(b)], and finally (iii) the Al-rich Al-Al-O-*R*-Al_2O_3 termination with Al in two octahedral sites [Al_1 and Al_0 in Fig. 4(b)]. In agreement with previous theoretical studies [14–18], our DFT calculations show that the Al-O-*R* termination is the most stable surface. However, at high temperatures and under oxygen deficient conditions corresponding to the experiment, other surface terminations with a higher Al content become accessible. This is illustrated in a phase diagram [Fig. 4(c)], where our DFT energies are combined with a thermodynamic model to calculate the surface-free energies for Al_2O_3 surfaces with increasing Al content as a function of sample temperature at a fixed oxygen partial pressure ($\sim 10^{-14}$ mbar). The calculations were done for a (1×1) Al_2O_3 unit cell to allow efficient screening of many structures. The Al-O-*R* structure is seen to be the most stable at temperatures up to $\sim$1700 K, where another termination consisting of a full Al layer on the Al-Al-O-*R* termination (3Al + Al-Al-O-*R*; see Fig. 4) has the lowest surface-free energy. This termination is obtained by desorbing the first two O layers of the stoichiometric Al_2O_3 termination, in which case four Al atoms are unconstrained per 1×1 unit cell and a close-packed Al layer is formed by three of them (3Al) and the last Al binds to the stoichiometric Al-O-*R* surface underneath resulting in the Al-Al-O-*R* substrate. Surprisingly, it is seen from Fig. 4(c) that filling of the "vacant" Al_3 sites of Al-Al-O-*R* in Fig. 4(b) (=Al-Al-Al-O-*R*) is found not to be favorable. Thus the DFT calculations predict that the experimental surface structure should be interpreted as a single Al layer on top of the Al-Al-O-*R* termination. Surfaces consisting of an Al layer on the oxygen terminated O-*R* surface corresponding to the model proposed in Ref. [19] were calculated to be unstable since free Al atoms spontaneously bind to the O-*R* surface and the Al-Al-O-*R* surface forms again.

As depicted in Fig. 4(b), the Al-Al-O-*R* surface contains three hexagonal sublattices with an average intersite distance of 2.75 Å defined by the high symmetry adsorption sites on either Al atoms (Al_1, Al_0, and vacant Al_3 positions), on-top O atoms (O_{top}), or the Al hollow sites with second layer O directly underneath (O_{sub}). Our DFT calculations show that the Al layer aligned on the Al hollow sites (O_{sub}) is more stable than adsorption on the on-top O positions (O_{top}) and Al positions which are higher in energy by 0.32 and 0.57 eV, respectively. However, the structure of the $\sqrt{31} \times \sqrt{31}R9°$ reconstructed surface visualized by nc-AFM is rotated and expanded to a periodicity of 3.01 Å compared to the average 2.75 Å of the sublattices of Al_2O_3. This implies that the stacking locally shifts between all sites of the Al-Al-O-*R* substrate resulting in the formation of the three categories domain pattern observed in Fig. 3. To explain the surprising fact that the Al atoms are distributed on all three types of sites and not only on the O_{sub} sites, we propose that a relief of strain energy in the Al overlayer compensates for the energy difference between the different low energy Al adsorption sites. Furthermore, we tentatively suggest that the lattice expansion and rotation, and hence the observed domain sizes and periodicity, are stabilized by an additional strain relief at the domain boundaries [21]. To directly confirm that the resulting stacking on different domains gives rise to the characteristic features observed in nc-AFM images,

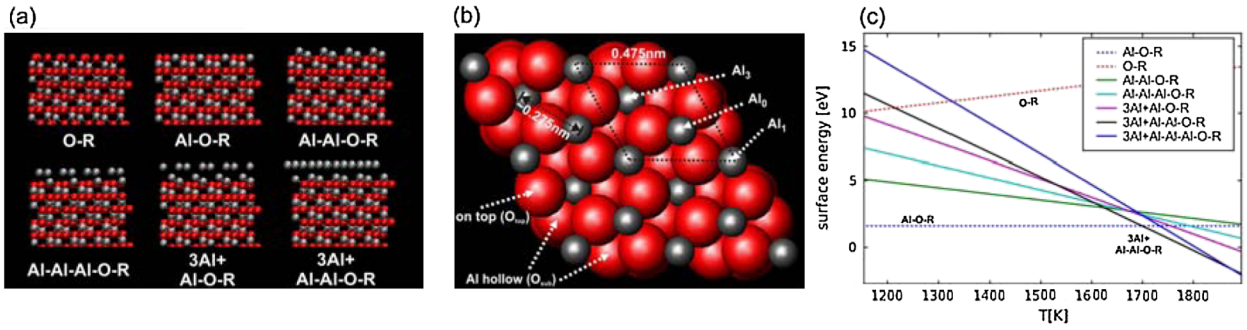

FIG. 4 (color online). (a) Calculated models (side view) of Al_2O_3 surface terminations with varying Al content. O (red) and Al (gray). The notation is (Al/unit cell in overlayer) + (substrate), e.g., 3Al + Al-Al-O-*R*. (b) Top view of the Al-Al-O-*R* termination of $Al_2O_3(0001)$. (c) Phase diagram for an O_2 pressure of 1×10^{-14} mbar. Energies were derived from DFT calculations for a 1×1 unit cell.

we have carried out elaborate calculations of the full $\sqrt{31} \times \sqrt{31}$ unit cell for the most stable configuration (3Al + Al-Al-O-*R*) including the underlying substrate with a slab thickness of two stoichiometric layers. In Fig. 2(c), we simulate the surface topography by plotting the relative vertical displacement of the surface Al atoms with the brown-white color scale of the experimental nc-AFM images. In the calculation we adopted the $[1\bar{1}0]\mathrm{Al}(111)/(R32°)[11\bar{2}0]\mathrm{Al_2O_3}$ epitaxial relationship found from the FT analysis as a starting configuration, and both the overlayer Al atoms and substrate atoms were allowed to relax both in-plane and perpendicularly to the surface. The lowest energy structure shown in Fig. 2(c) indeed contains the three subdomains superimposed on the $\sqrt{31} \times \sqrt{31}R9°$ superstructure with the same domain size, symmetry, shape, and rotation as observed experimentally. As illustrated in the lower part of Fig. 3, the Al atoms are each locally commensurate with a set of equivalent adsorption sites on the Al-Al-O-*R* substrate layer. Domain **1** is composed of Al atoms placed near the on-top position of O atoms (O_{top}) of the Al-Al-O-*R* substrate. The symmetry of this domain is characterized by three slightly shifted, four-atom-wide triangles with a rotated baseline and a bright center, in agreement with the experiment. Domain **2** (on-top Al) consists of Al surface atoms placed at on-top Al sites, but since only Al_1 and Al_0 sites are occupied in Al-Al-O-*R*, the single Al atoms placed near the vacant (Al_3) sites relax ~0.3 Å inwards and generate a ''hexagonal'' six-membered ring feature. In excellent agreement with the experiment, four of these ''hexagons'' appear in a *Y* shape around the site where the Al layer is exactly commensurate with the Al positions. The last option reflects Al atoms placed near the hollow sites and accounts for domain **3** (O_{sub}), and again the shape, size, and orientation of the triangle feature outlined by atoms placed near hollow sites are in good accordance with the experiment.

Periodic superstructures formed by lattice mismatch is a classic phenomenon observed previously for, e.g., metal on metal growth [22,23] or for thin films [24,25], and the present $\sqrt{31} \times \sqrt{31}R9°$ structure for the insulating aluminum surface bears resemblance to such systems, with the unusual exception that three preferential types of substrate sites are involved. For comparison, the isostructural α-$Fe_2O_3(0001)$ surface is predicted to be Fe-O-*R* terminated like the Al-O-*R* surface of this study [26], and upon reduction the existence of well-defined surface structures with varying Fe^{3+} and Fe^{2+} content have also been revealed [27,28]. The results of this nc-AFM study can be compared with previous structural information for the $\sqrt{31} \times \sqrt{31}R9°$ structure based on surface x-ray diffraction [19] and previous atom-resolved AFM studies of the same structure which showed a slight degree of disorder at the unit cell boundaries [6]. However, it should be noted that our proposed model differs in a significant way as the overlayer is observed to be completely well-ordered. A detailed understanding of the surface chemistry and physics of insulating metal oxides is, in general, of utmost importance in a variety of different areas, such as heterogeneous catalysis and for ceramic coatings, and the nc-AFM/DFT approach presented here should have general applicability to the full range of insulating ceramic surfaces.

J. V. L. and iNANO gratefully acknowledge financial support from the Lundbeck Foundation and Haldor Topsøe A/S. Furthermore, we acknowledge the financial support for the NABIIT Project No. 2106-06-0016.

*Corresponding author.
jvang@inano.dk

[1] K. Wefers and M. Chanakya, Alcoa Technical Paper No. 19, 1987, revised.
[2] J. Toofan and P. R. Watson, Surf. Sci. **401**, 162 (1998).
[3] T. M. French and G. A. Somorjai, J. Phys. Chem. **74**, 2489 (1970).
[4] S. Morita, R. Wiesendanger, and E. Meyer, *Noncontact Atomic Force Microscopy* (Springer, New York, 2002).
[5] F. J. Giessibl, Rev. Mod. Phys. **75**, 949 (2003).
[6] C. Barth and M. Reichling, Nature (London) **414**, 54 (2001).
[7] C. C. Chang, J. Appl. Phys. **39**, 5570 (1968).
[8] I. Vilfan *et al.*, Surf. Sci. **505**, L215 (2002).
[9] J. Wang *et al.*, Surf. Sci. **515**, 337 (2002).
[10] G. H. Enevoldsen *et al.*, Phys. Rev. B **76**, 205415 (2007).
[11] The open-source DFT code DACAPO is available at http://www.camd.dtu.dk/Software.aspx.
[12] D. Vanderbilt, Phys. Rev. B **41**, 7892 (1990).
[13] B. Hammer, L. B. Hansen, and J. K. Nørskov, Phys. Rev. B **59**, 7413 (1999).
[14] B. Hinnemann and E. A. Carter, J. Phys. Chem. C **111**, 7105 (2007).
[15] X. G. Wang, A. Chaka, and M. Scheffler, Phys. Rev. Lett. **84**, 3650 (2000).
[16] Z. Lodziana and J. K. Nørskov, J. Chem. Phys. **115**, 11 261 (2001).
[17] E. A. A. Jarvis and E. A. Carter, J. Phys. Chem. B **105**, 4045 (2001).
[18] K. C. Hass *et al.*, Science **282**, 265 (1998).
[19] G. Renaud *et al.*, Phys. Rev. Lett. **73**, 1825 (1994).
[20] We note that a rotation of $23 - 9 = 14$ degrees did not yield a commensurate superstructure with the correct dimensions.
[21] D. Vanderbilt, Surf. Sci. **268**, L300 (1992).
[22] H. Brune *et al.*, Nature (London) **394**, 451 (1998).
[23] K. Pohl *et al.*, Nature (London) **397**, 238 (1999).
[24] M. Corso *et al.*, Science **303**, 217 (2004).
[25] G. Kresse *et al.*, Science **308**, 1440 (2005).
[26] E. A. Jarvis and A. M. Chaka, Surf. Sci. **601**, 1909 (2007).
[27] N. G. Condon *et al.*, Phys. Rev. Lett. **75**, 1961 (1995).
[28] X.-G. Wang *et al.*, Phys. Rev. Lett. **81**, 1038 (1998).